Investigation of Short-Time Isomerization Dynamics in *p*-Nitroazobenzene from Resonance Raman Intensity Analysis

Nandita Biswas,† Becky Abraham, and Siva Umapathy*,‡

Department of Inorganic and Physical Chemistry, Indian Institute of Science, Bangalore-560012, India

Received: March 1, 2001; In Final Form: July 11, 2002

Resonance Raman (RR) spectra are presented for *p*-nitroazobenzene dissolved in chloroform using 18 excitation wavelengths, covering the region of $^1(n \rightarrow \pi^*)$ electronic transition. Raman intensities are observed for various totally symmetric fundamentals, namely, C−C, C−N, N═N, and N−O stretching vibrations, indicating that upon photoexcitation the excited-state evolution occurs along all of these vibrational coordinates. For a few fundamentals, interestingly, in *p*-nitroazobenzene, it is observed that the RR intensities decrease near the maxima of the resonant electronic $^1(n \rightarrow \pi^*)$ transition. This is attributed to the interference from preresonant scattering due to the strongly allowed $^1(\pi \rightarrow \pi^*)$ electronic transition. The electronic absorption spectrum and the absolute Raman cross section for the nine Franck−Condon active fundamentals of *p*-nitroazobenzene have been successfully modeled using Heller's time-dependent formalism for Raman scattering. This employs harmonic description of the lowest energy $^1(n \rightarrow \pi^*)$ potential energy surface. The short-time isomerization dynamics is then examined from a *priori* knowledge of the ground-state normal mode descriptions of *p*-nitroazobenzene to convert the wave packet motion in dimensionless normal coordinates to internal coordinates. It is observed that within 20 fs after photoexcitation in *p*-nitroazobenzene, the N═N and C−N stretching vibrations undergo significant changes and the unsubstituted phenyl ring and the nitro stretching vibrations are also distorted considerably.

Introduction

With the availability of tunable lasers, resonance Raman (RR) spectroscopy has become a commonly used technique to probe the structure and dynamics of short-lived excited-state intermediates of various photochemical and photophysical processes.[1−15] Although, electronic spectroscopy may also be useful in providing information about the lifetime and decay rates of the excited states in polyatomic molecules, it often lacks vibrational mode-specific information because of its unresolved and unstructured envelope in the condensed phase, especially at room temperature (RT). Thus, to extract valuable excited-state structural information present in a polyatomic molecule, RR spectroscopic technique is normally used.

Under preresonance or resonance conditions, that is, when the excitation wavelength approaches or coincides with a particular electronic transition of the system under investigation, the RR spectra show enormous intensity enhancement. This essentially contains information about the excited-state potential energy surface and hence, in turn, can dictate the initial dynamics of nuclear motion in the Franck−Condon (FC) region of the potential energy surface. Such dynamical processes following photoexcitation from the ground to the resonant excited electronic state within the electronic dephasing time can be intuitively understood through Heller's time-dependent formalism for Raman scattering.[16]

Wavelength dependence of the Raman scattering intensity, namely, Raman excitation profiles (REPs), provides valuable information on the origin of RR intensities and also the dynamics associated with the resonant excited state.[11−14] Qualitatively, if the vibrational modes are FC active in the resonant electronic state then the Raman intensities are enhanced for these modes because of A-term Raman scattering.[17−19] Therefore, the REPs of these vibrational modes are expected to follow the shape of the absorption spectrum corresponding to the electronic state to which the resonance excitation is carried out. The REPs thus carry mode-specific information about the excited-state potential energy surface in the FC region. The knowledge of absolute Raman intensities is essential to provide a complete characterization of the excited-state potential energy surface and to know the extent of homogeneous and inhomogeneous broadening contributions. Occasionally, the REPs do not follow the shape of the absorption spectrum; instead, antiresonance or deenhancement may be observed for the totally symmetric vibrational modes because of interference[14c,d,15,20−33] from electronic states lying at higher energies as compared to the resonant electronic state. Thus, destructive interference between a pair of Raman polarizability tensors having different sources of origin, namely, the FC activity corresponding to resonant electronic state and the vibronic activity arising because of preresonant electronic state, results in deviation from the expected excitation profiles.

Azo dyes find extensive applicability in analytical chemistry as acid−base, redox and, metallochromic indicators. They also find wide applicability for reversible optical data storage[34−37] (both holographic and digital). Optical data storage has been demonstrated with several liquid-crystalline and amorphous polymers having azo dyes either covalently attached[38−41] or dissolved.[42] The storage process utilizes the light-induced trans−cis−trans isomerization of the azo dyes, thereby using the local

* To whom correspondence should be addressed. E-mail: umapathy@ipc.iisc.ernet.in; suma@hamsadvani.serc.iisc.ernet.in. Fax: -91-80-3601552.

† Present address: Department of Chemical Sciences, Tata Institute of Fundamental Research, Homi Bhabha Road, Colaba, Mumbai-400005, India.

‡ Swarna Jayanthi Fellow.

10.1021/jp0108162 CCC: $22.00
Published on Web 09/18/2002

variation of the refractive index of the medium, which is sufficient for holographic recording. The photoinduced change in polarity and molecular structure have led to widespread application of azobenzene derivatives as reversible molecular switching devices.[43−47] Because of their wide applicability, mainly due to the photoisomerization phenomenon,[48] the azo dyes have been extensively studied both experimentally[14,48−53] and theoretically,[54] yet the dynamics of their excited states are not well understood. This is mainly because the absorption spectra of these azo dyes are poorly resolved even at low temperatures.[55] Investigation of the excited-state properties of the azo dyes has been difficult because neither the cis nor the trans isomers exhibit fluorescence emission.[56] This lack of fluorescence is believed to result from an extremely short lifetime of the excited state.[50a,b]

In this paper, we have analyzed the RR intensities for the FC active vibrations of *p*-nitroazobenzene dissolved in chloroform to understand the short-time dynamics associated with photoisomerization (vide infra) on resonant $^1(n \rightarrow \pi^*)$ excitation. We have measured the intensities of the Raman active modes in resonance to the $^1(n \rightarrow \pi^*)$ electronic transition, utilizing 18 excitation wavelengths. A theoretical simulation of RR intensities under the $^1(n \rightarrow \pi^*)$ absorption envelope has been carried out using Heller's time-dependent wave packet formalism for RR scattering.[16] From the RR intensity analysis, we have presented qualitative evidence for an inversion mechanism as the isomerization pathway under the excitation resonant to the lowest-energy transition. An examination of the REPs for the vibrational modes of *p*-nitroazobenzene displays de-enhancement near the maxima corresponding to the lowest energy $^1(n \rightarrow \pi^*)$ electronic transition for five fundamentals, namely, 1449, 1413, 1180, 1143, and 1109 cm^{-1}. The observed de-enhancement indicates that the resonant electronic state is not the sole source of intensity for these fundamental vibrations and can be attributed to the interference from excited electronic states lying higher in energy (preresonant electronic state) as compared to the resonant electronic state. The main objective of this study is to provide a detailed mode-specific picture of the initial stages of short-time isomerization dynamics near the FC region of the excited electronic potential energy surface in *p*-nitroazobenzene. Combining the results obtained from Heller's time-dependent wave packet analysis of the experimental RR intensities with the inclusion of interference effect from the preresonant electronic state and the knowledge of normal mode descriptions, we have been able to elucidate the ultrafast dynamical information along various vibrational coordinates. The conversion of the dimensionless displacements derived from wave packet dynamical study to internal coordinates help in visualization of the distortions in the molecular structure during the initial stages of isomerization dynamics.

Experimental Methods

The excitation wavelengths for the Raman experiments in the visible region, namely, 440, 443, 452, 461, 470, 480, 492, 501, 510, 522, 532, 541, 550, 560, 572, 581, 590, and 600 nm, were scanned using a tunable laser pulse output from an optical parametric oscillator (OPO) (MOPO 730, Spectra Physics). The OPO was pumped by the third harmonic (355 nm) of a 10 Hz Q-switched Nd:YAG laser (GCR 250, Spectra Physics) providing a high-energy laser pulse of 560 mJ. The energy of the OPO output was in the range of 5−10 mJ/pulse. A SPEX 1404 double monochromator was used with two 600 groove gratings blazed at 500 nm to disperse the scattered light. A liquid nitrogen cooled charge coupled device (Princeton Instruments) with 576 × 378 pixels was used as the multichannel detector. The recorded Raman spectra were calibrated using known solvent bands as reference, and the spectral resolution was estimated to be 5 cm^{-1}. The Raman signal was found to be linear with laser power, and all of the observed Raman bands were found to arise from the trans isomer.

p-Nitroazobenzene used in the Raman measurements was purchased from Aldrich Chemical Co. and used as received. Chloroform ($CHCl_3$) was of analytical grade and used as received. Freshly prepared sample solutions of *p*-nitroazobenzene in $CHCl_3$ were circulated through a capillary at the rate of about 10 mL/min. These solutions were used in the dark for each Raman measurement. In *p*-nitroazobenzene, because the excited state is short-lived, during a nanosecond laser pulse, the molecule might photoisomerize. The amount of the cis isomer in the solution, which is produced by photoisomerization, is negligibly small because the cis isomer thermally returns to the trans form with a time constant as short as 50 μs.[50c] Hence, the irradiated solution of *p*-nitroazobenzene mainly consisted of the trans isomer. This was checked routinely after each Raman measurement by UV−visible absorption, as well as vibrational spectroscopy, because the cis and trans isomers have distinguishable absorption, as well as vibrational spectra.

Using a 180° backscattering collection geometry minimizes the reabsorption of the RR scattered light by the sample. Remaining reabsorption of the Raman scattered light by the sample was corrected using the methods described previously.[13,57,58] The sample concentration used for Raman experiments was about 5×10^{-2} M. Thus, the absolute Raman cross sections for *p*-nitroazobenzene in $CHCl_3$ were determined relative to the absolute intensities of the $CHCl_3$, 1218 cm^{-1} band.[14e,f]

Theory and Computational Methods

On photoexcitation of a molecule to a particular electronic level, it is assumed, in general, that the enhancement in RR intensity arises solely because of the resonant electronic state, and hence, the REPs are expected to follow the electronic absorption band profile. But in practice, occasionally, as is observed in the present study, there may be a decrease in Raman intensities as the excitation wavelength is tuned toward the absorption maximum. Such a de-enhancement[14c,d,15,20−33] in RR intensities may arise because of the interference from electronic states other than the resonant excited state termed as preresonant electronic states. The interference effects are normally controlled by various factors[30] such as the energy gap between the resonant and interfering (preresonant) electronic states, the transition dipole moments of the two electronic states, nature (spin state, symmetry, and polarization) of the two states involved, and the extent of vibronic coupling between them. In the present study, we have modeled the experimental REPs for the fundamental vibrations of *p*-nitroazobenzene taking into consideration the resonance and preresonance interference effects.[15]

Heller's time-dependent wave packet approach to RR scattering[16] is used to simulate the absorption spectrum and the absolute Raman intensities of *p*-nitroazobenzene in $CHCl_3$ solution. In the time-dependent picture, an initial wave packet, $|i\rangle$, in the zeroeth vibrational state of the ground electronic level is transported to the excited electronic level, where it evolves in time under the influence of the excited-state Hamiltonian (H_{ex}). This time-evolving wave packet, $|i(t)\rangle$, which is moving away from the FC region with time "*t*", is transposed back to the ground electronic level at various intervals of time and overlapped with different vibrational levels, $|i\rangle$ or $|f\rangle$ (vibrational

states other than zeroeth state), resulting in the autocorrelation, $\langle i|i(t)\rangle$, or the Raman correlation, $\langle f|i(t)\rangle$, function, respectively. The absorption spectrum is essentially the full Fourier transform of the autocorrelation function, and thus, the electronic absorption spectrum of *p*-nitroazobenzene for the $^1(n \rightarrow \pi^*)$ transition can be expressed as[11,13]

$$\sigma_A = \frac{4\pi e^2 M^2 E_L}{3\hbar^2 cn}\int_{-\infty}^{\infty}\langle i|i(t)\rangle \exp\left[\frac{i(E_L + E_i)t}{\hbar} - g(t)\right] dt \quad (1)$$

where E_L is the incident photon energy, E_i is the zero-point vibrational energy in the ground state, n is the solvent refractive index ($CHCl_3 = 1.445$), M is the electronic transition dipole evaluated at the equilibrium geometry, e is the charge of an electron, $\hbar = h/(2\pi)$ (h being Planck's constant), and c is the velocity of light.

On the other hand, the half Fourier transform of the Raman correlation function results in RR amplitudes,[11,13] α_{res}, and is given by

$$\alpha_{res} = \frac{(eM^2)}{\hbar}\int_0^{\infty}\langle f|i(t)\rangle \exp\left[\frac{i(E_L + E_i)t}{\hbar} - g(t)\right] dt \quad (2)$$

Thus, the RR cross section resulting from the lowest excited $^1(n \rightarrow \pi^*)$ electronic transition can be obtained as

$$\sigma_R(E_L,E_S) = \frac{8\pi {E_S}^3 E_L}{9\hbar^4 c^4}|\alpha_{res}|^2 \quad (3)$$

where E_s is the energy of the scattered photon.

The time-evolving wave packet,[16] $|i(t)\rangle$, on the excited-state surface is expressed as

$$|i(t)\rangle = \exp\left(-\frac{iH_{ex}t}{\hbar}\right)|i\rangle \quad (4)$$

where $\exp(-iH_{ex}t/\hbar)$ is the time-evolution operator. The time evolution of the wave packet is carried out using the grid technique.[59,60] This evolving wave packet, $|i(t)\rangle$, during its motion on the excited-state potential is damped by the function $\exp[-g(t)]$, which includes both lifetime broadening (Γ) and the possibility of relaxation into other modes, including the bath, which is usually modeled by a Gaussian decay, $\exp[-\beta^2t^2/(2\hbar^2)]$. Thus,

$$\exp[-g(t)] = \exp\left(-\frac{\Gamma t}{\hbar}\right)\exp\left(-\frac{\beta^2 t^2}{2\hbar^2}\right) \quad (5)$$

To introduce the effect of interference arising from the preresonant electronic states, we have used the single-state A-term frequency dependence[17,61] as a first approximation. Thus, the Raman cross section corresponding to the preresonant electronic state is expressed as

$$\sigma_R(E_L,E_S) = E_L {E_S}^3 \{A_{pre}\}^2 \quad (6)$$

$$\{A_{pre}\}^2 = K\left[\frac{{E_e}^2 + {E_L}^2}{({E_e}^2 - {E_L}^2)^2}\right]^2 \quad (7)$$

where E_e is the energy corresponding to the preresonant electronic state and K represents the strength of coupling of the Raman transition to the preresonant electronic state.

In *p*-nitroazobenzene, similar to the case of the parent molecule, azobenzene, the electronic transitions are partially localized about the central N=N bond,[62] thus giving rise to two different components of the Raman polarizability tensor, namely, $\alpha_{||}$ and $\alpha_{\perp}$ (transition parallel and perpendicular to the N=N axis, respectively). As observed from the magnetic circular dichroism studies,[63] the lowest-lying electronic absorption band in *p*-nitroazobenzene is polarized perpendicular to the N=N axis, implying that the resonant electronic state contributes only to $\alpha_{\perp}$ term of the Raman polarizability tensor. The higher-lying electronic absorption band consists of two components: one (major component) corresponds to the transition parallel to the N=N axis, while the other (minor component) is perpendicular to the N=N axis. Thus, there are two different possibilities by which the resonant and the preresonant terms can interfere.[15] The first possibility of interference between the resonant and the preresonant polarizability tensors arises when both the resonant and the preresonant terms are polarized along the same direction (viz., perpendicular to the N=N axis) thus contributing to the same component of transition polarizability tensor, $\alpha_{\perp}$. The measured value of depolarization ratio (ρ) in this case is a constant and independent of the excitation wavelength. The Raman cross section resulting because of this kind of resonance and preresonance interference[15] is expressed as follows:

$$\sigma_R(E_L,E_S) = \frac{8\pi {E_S}^3 E_L}{9\hbar^4 c^4}|\alpha_{res} + \alpha_{pre}|^2 \quad (8)$$

where α_{pre} is related to the A_{pre} term by the expression

$$|\alpha_{pre}|^2 = \frac{9\hbar^4 c^4}{8\pi}\{A_{pre}\}^2 \quad (9)$$

The second possibility of interference occurs when the preresonant term of the polarizabilty tensor contributes to $\alpha_{||}$ (viz., the transition is polarized parallel to the N=N axis), where as the resonant term contributes to $\alpha_{\perp}$, that is, the electronic states are polarized perpendicular to each other. In this particular case, the depolarization ratio (ρ) is not a constant; instead, it is a function of the excitation wavelength.[15]

The preresonant contribution to the polarizability is assumed to be purely imaginary. This is because the resonant term (α_{res}) tends to an imaginary quantity as the excitation wavelength is tuned away from the resonance region. Not only the magnitude of the changes in normal coordinates is of importance, but also the direction of its change is of major significance. The actual direction of geometry change along a particular normal coordinate determines the relative sign of the polarizability in the resonant and the preresonant electronic states. In the case of *p*-nitroazobenzene, the optical properties are found to be similar to those of the parent azobenzene molecule.[63] Hence, it is expected that photoexcitation into the lowest energy $^1(n \rightarrow \pi^*)$ electronic transition leads to isomerization via inversion. This is confirmed from the magnitude of dimensionless displacements along various normal coordinates. This is in contrast to the photoexcitation into the strongly allowed $^1(\pi \rightarrow \pi^*)$ electronic transition, resulting in isomerization via rotation. During the process of inversion, one of the N lone pair dipoles of the −N=N− group is converted to a p orbital, that is, rehybridization from the sp^2 to the sp state occurs. Thus, inversion leads to a decrease in N=N bond order and, hence, an increase in N=N bond length. On the other hand, rotation of the molecule about the N=N bond involves scission of the double bond to a single bond, resulting in a biradical structure. Hence, rotation also leads to an increase in azo bond length and a decrease in the C−N bond. This fact is supported from the study of excited-state geometry changes in bacteriorhodopsin, in which all of

the double bonds elongate and all single bonds undergo reduction upon photoexcitation.[64]

In the present study, the ground- and excited-state potential energy surfaces are approximated as harmonic oscillators with the excited-state potential energy minima displaced by an amount, Δ (in dimensionless units), relative to the ground-state minimum. The magnitudes of the dimensionless displacement parameters are obtained as an initial estimate from the experimental RR intensities assuming short-time dynamics[16] (i.e., Raman intensity, $I_R \propto \Delta^2\omega^2$). This is reasonable because we are interested only in the FC region of the total potential energy surface. Moreover, the low-temperature absorption spectrum of *p*-nitroazobenzene shows no structure.[55] The dimensionless displacements for the respective modes are obtained at all of the excitation wavelengths from the experimental Raman intensities relative to the intensity for the 1602 cm^{-1} band. The average dimensionless displacement for the respective Raman active mode is then calculated and fed into our simulations for the absorption spectrum and the Raman excitation profiles. This procedure is repeated several times for various values of dimensionless displacements to get minimum deviation for the simulated absorption spectrum and the Raman excitation profiles in comparison to the respective experimental spectrum. Thus, the best fit value for the displacement, Δ, corresponding to each Raman active vibration is obtained. In our simulations, coordinate dependence of the transition length, as well as Duschinsky mixing of the normal coordinates, is not taken into consideration.

After photoexcitation, the center of the wave packet undergoing separable harmonic motion at time t is expressed in dimensionless normal coordinates[15] as

$$q_\alpha(t) = \Delta_\alpha(1 - \cos \omega_\alpha t) \tag{10}$$

where $q_\alpha = 0$ for all of the normal modes α at zero time when the molecule is at ground-state equilibrium position and ω_α ($= \varpi_\alpha/5308.8$, ϖ_α is the frequency in cm^{-1} and 5308.8 corresponds to the value of $\hbar$ in units of cm^{-1} fs) is the vibrational frequency in fs^{-1}. To visualize the short time isomerization dynamics in terms of internal coordinate changes, we have converted the dimensionless normal coordinate displacement, $\{q_\alpha(t)\}$, to the internal coordinate displacement, $\{S_i(t)\}$, by the following expression:[15]

$$S_i(t) = \left(\frac{\hbar}{c}\right)^{1/2} \sum_\alpha A_{\alpha i} \varpi_\alpha{}^{-1/2} q_\alpha(t) \tag{11}$$

where, $S_i(t)$ is the change in internal coordinates, namely, stretches, bends, torsions, wags, etc. (as defined by Wilson, Decius, and Cross[65]), at time t with respect to the ground-state equilibrium geometry and $A_{\alpha i}$ is the normal mode coefficient ($\delta S_i/\delta Q_\alpha$) and is obtained from normal coordinate analysis (Q_α being the normal coordinate) via the unitary transformation,[11,13]

$$\mathbf{AFA}^+ = \mathbf{\Lambda} \tag{12}$$

where the matrix **A** represents the normal mode vectors and the diagonal matrix $\mathbf{\Lambda}$ represents the eigenvalues. The potential energy matrix, **F**, is obtained from the valence force field[66] at the ground-state equilibrium geometry for *p*-nitroazobenzene, which is computed employing the density functional method, B3LYP with 6-31G basis set using the Gaussian 94 package.[67] B3LYP with 6-31G is found to be very accurate in predicting vibrational frequencies and, therefore, the force field for polyatomic systems.[66,68]

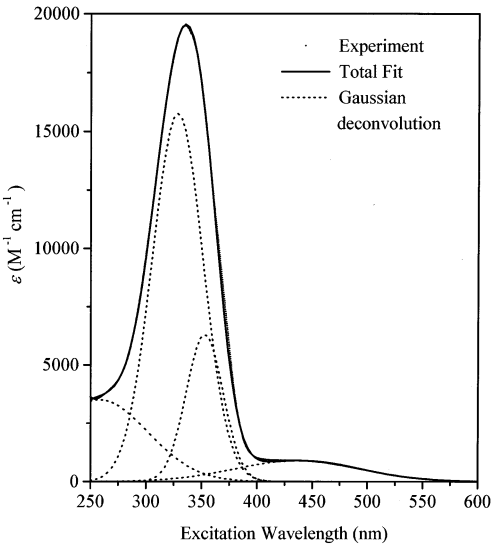

Figure 1. Absorption spectrum of *p*-nitroazobenzene in chloroform. The weak band from 400 to 600 nm corresponds to the $^1(n \rightarrow \pi^*)$ electronic transition, and the strong band in the region 250−400 nm is due to the $^1(\pi \rightarrow \pi^*)$ transition.

Results and Discussion

p-Nitroazobenzene exhibits planar structure (C_s symmetry) in solution with 72 fundamentals spanning the representation $\Gamma = 49A' + 23A''$ vibrations.[66] All of the fundamental modes are both Raman and infrared (IR) active. The electronic absorption spectrum of *p*-nitroazobenzene consists of a lowest-energy symmetry-forbidden $^1(n \rightarrow \pi^*)$ transition, in addition to the strongly allowed $^1(\pi \rightarrow \pi^*)$ transition. On resonance excitation to the $^1(n \rightarrow \pi^*)$ electronic transition, Raman bands are expected to be observed for the vibrational modes that are FC active for this particular transition, and one would also expect the vibrational modes to follow the electronic absorption spectrum. But in the present study, it is observed that the REPs for various vibrations do not follow the absorption spectrum; rather, it shows a decrease in intensity near its maxima. This decrease in intensity in the REPs may be attributed to the destructive interference among the transition polarizability components in the resonant and preresonant electronic states. Detailed analyses of the experimental and simulated absorption spectrum, as well as the REPs, are carried out in sections A−D.

A. Absorption Spectrum. The absorption spectrum of *p*-nitroazobenzene in $CHCl_3$ is shown in Figure 1. The spectrum exhibits two distinct features. The most intense feature appearing around 335 nm corresponds to the strongly allowed $^1(\pi \rightarrow \pi^*)$ electronic transition, and the weak feature with a peak at 437 nm represents the symmetry-forbidden $^1(n \rightarrow \pi^*)$ transition. It is evident from the figure that the asymmetry appearing in the intense feature around 335 nm cannot be simulated by a single Gaussian. Thus, the absorption spectrum is deconvoluted into a sum of four Gaussian components, as shown in the figure, to estimate the strength and position of the $^1(n \rightarrow \pi^*)$ and the $^1(\pi \rightarrow \pi^*)$ electronic transitions. The absence of vibrational structure in the low-temperature absorption spectrum[55] corresponding to the $^1(n \rightarrow \pi^*)$ transition of *p*-nitroazobenzene implies that isomerization occurs much more rapidly than the vibrational recurrences to the FC region.

B. Resonance Raman (RR) Spectra. The Raman spectra of *p*-nitroazobenzene in $CHCl_3$ resonant with the $^1(n \rightarrow \pi^*)$ electronic transition are recorded using various excitation wavelengths, namely, 440, 443, 452, 461, 470, 480, 492, 501, 510, 522, 532, 541, 550, 560, 572, 581, 590, and 600 nm. For

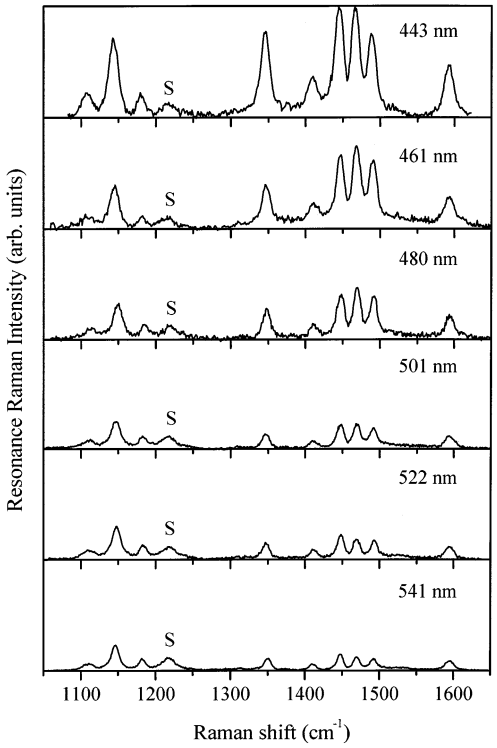

Figure 2. Resonance Raman spectra of *p*-nitroazobenzene in chloroform with excitation wavelengths 443, 461, 480, 501, 522, and 541 nm.

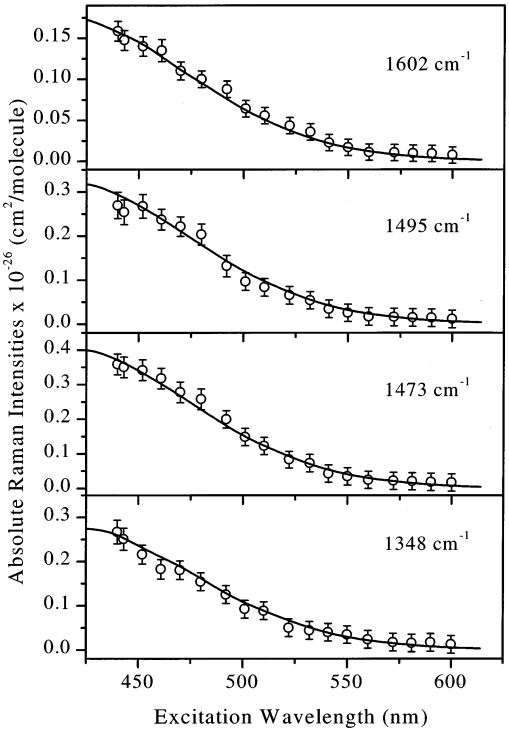

Figure 3. The experimental (open circles) and the simulated (solid line) Raman excitation profiles for 1602, 1495, 1473, and 1348 cm^{-1} vibrations of *p*-nitroazobenzene.

the sake of brevity, the Raman spectra at a few excitation wavelengths, 443, 461, 480, 501, 522, and 541 nm, are shown in Figure 2. The spectra at all wavelengths are normalized with respect to the solvent, $CHCl_3$, band (marked S in the figure) appearing at 1218 cm^{-1}. The fundamentals observed in the region 1000−1600 cm^{-1} are 1109, 1143, 1180, 1348, 1413, 1449, 1473, 1495, and 1602 cm^{-1}. The most intense Raman bands appear at 1449, 1473, 1495, 1348, and 1143 cm^{-1} and are followed by a 1602 cm^{-1} band of medium intensity. Three weak bands are observed at 1109, 1180, and 1413 cm^{-1}. It is clear from the figure that the intensities of various fundamentals vary significantly as a function of the excitation wavelength.

To investigate the changes in intensities with the excitation wavelength, we plot the REPs of the fundamentals in Figures 3 and 4. The open circles represent the experimentally observed REPs of various modes. In Figure 3, the REPs for the 1602, 1495, 1473, and 1348 cm^{-1} vibrations are displayed. It is observed that as the excitation wavelength approaches the lowest resonant energy transition [viz., $^1(n \rightarrow \pi^*)$], with λ_{max} at 437 nm, the intensities of the fundamental modes increase monotonically and the shape of the REPs follow the absorption spectral profile as expected. Resonance enhancement of these Raman fundamentals is supported by the observation of very weak overtones and combination bands at a few excitation wavelengths, namely, 443 and 480 nm. In contrast, the REPs corresponding to the fundamental vibrations, namely, 1109, 1143, 1180, 1413, and 1449 cm^{-1}, as shown in Figure 4 exhibit de-enhancement in intensity as the excitation wavelength is tuned toward the maximum of the $^1(n \rightarrow \pi^*)$ electronic transition. The observation of resonance de-enhancement in these vibrations indicates that the Raman intensities corresponding to these FC active modes not only arise because of the lowest-energy resonant electronic state but also have contributions from higher-lying excited electronic states.

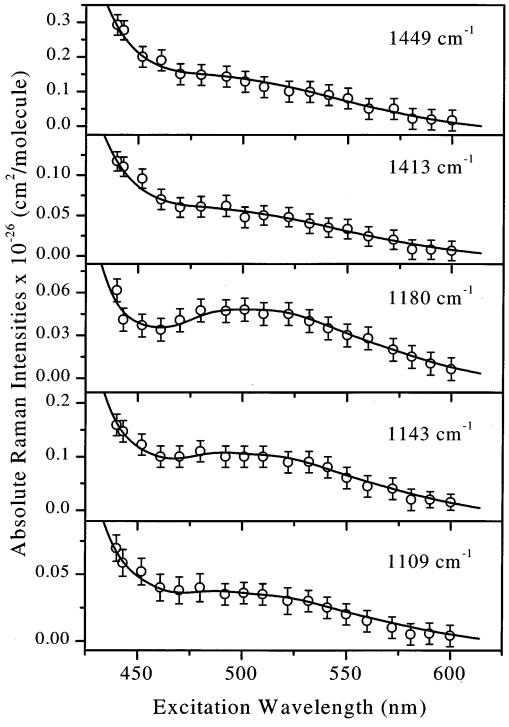

Figure 4. The experimental (open circles) and the simulated (solid line) Raman excitation profiles for 1449, 1413, 1180, 1143, and 1109 cm^{-1} vibrations of *p*-nitroazobenzene.

To account for the effect of interference from the preresonant electronic state corresponding to the $^1(\pi \rightarrow \pi^*)$ electronic transition with maxima near 335 nm into the resonant polarizability component, the depolarization ratios (ρ) are measured as a function of the excitation wavelength and are presented in Table 1. The resonance Raman depolarization ratios at excitation wavelengths 443, 480, and 522 nm are measured for the

TABLE 1: Depolarization Ratios for the Normal Raman Vibrations of *p*-Nitroazobenzene at the Excitation Wavelengths of 443, 480, and 522 nm

vibrational mode	frequency (ω in cm^{-1})	depolarization ratio[a]		
		443 nm	480 nm	522 nm
υ_7	1602	0.33	0.37	0.40
υ_8	1495	0.26	0.32	0.39
υ_9	1473	0.30	0.36	0.39
υ_{10}	1449	0.26	0.36	0.37
υ_{12}	1413	0.37	0.37	0.35
υ_{13}	1348	0.29	0.35	0.30
υ_{15}	1180	0.28	0.38	0.33
υ_{18}	1143	0.37	0.39	0.29
υ_{19}	1109	0.30	0.32	0.28

[a] Error bar = ±0.06; Error bar represents standard deviation from the mean.

fundamental transitions. The depolarization ratio (ρ) is defined as the intensity of the scattered light observed with polarization perpendicular to the polarization of the excitation light divided by the intensity of the observed scattering light with polarization parallel to the incident light. The intensities of the Raman scattered light with polarization perpendicular and parallel to that of the incident light are measured by both simple peak integration and by fitting the Raman transitions with Lorentzian convolution. The measured values of the depolarization ratios are found to be nearly constant (0.33 ± 0.06) and independent of the excitation wavelength. This implies that the preresonant electronic state contributes to the same component of the transition polarizability tensor ($\alpha_\perp$) as does the resonant electronic state (as discussed previously in the section of Theory and Computational Methods). Thus, in our simulations, we assume that both the preresonant and the resonant electronic states are polarized perpendicular to the N=N axis. This is also supported by the magnetic circular dicroism results on *p*-nitroazobenzene.[63] The sign of the transition polarizability tensor depends on the direction of the actual change in geometry occurring along a particular normal coordinate. As discussed earlier, in the present study, we assume that the signs of the transition polarizability for *p*-nitroazobenzene remain similar to those of azobenzene.[14c] This is a reasonable assumption because the substitution by a nitro group at the para position in one of the benzene rings is not expected to change drastically the spectral properties of the molecule. The absorption and the magnetic circular dichroism results[63] of both compounds further support this. The effect of interference in the fundamental modes, namely, 1449, 1413, 1180, 1143, and 1109 cm^{-1}, is introduced in our simulations by assuming the polarizability tensor elements ($\alpha_\perp$) for these modes to be opposite in sign in the resonant and the preresonant electronic states.

C. Simulation of the Raman Excitation Profiles (REPs) and the Absorption Spectrum. The excitation profiles for the nine Raman active fundamental modes are simulated using eqs 2−5. Solid lines in Figure 3 show the simulated REPs obtained for the fundamental modes undergoing no de-enhancement. A good agreement between the experimental and the simulated curve is clearly observed in the figure. Solid lines in Figure 4 show the simulated REPs for the modes undergoing resonance de-enhancement. In the simulations for the modes undergoing resonance de-enhancement, the contribution from the preresonant electronic state (eqs 6−9) has been taken into account. As stated earlier, the preresonant component of the polarizability tensor is introduced as A-term frequency dependence[17,61] with two fitting parameters, namely, the strength of coupling of the Raman transition to the preresonant electronic state (K) and the energy corresponding to the preresonant electronic state (E_e). The parameters related to the preresonant component are E_e = 30 500 cm^{-1} and K = 0.52 ± 0.24, 0.21 ± 0.09, 0.07 ± 0.03, 0.27 ± 0.12, and 0.11 ± 0.05 mb (1 mb = 10^{-27} cm^2) for the modes 1449, 1413, 1180, 1143, and 1109 cm^{-1}, respectively. The fits to the experimental REPs are remarkable. The transition polarizability component in this case, due to the preresonant electronic state (α_{pre}), has significant magnitude when extrapolated to the resonant electronic state. The introduction of destructive interference between a preresonance term (due to the strongly allowed $^1(\pi \rightarrow \pi^*)$ electronic transition) and a rigorous resonance term (due to the symmetry-forbidden $^1(n \rightarrow \pi^*)$ electronic transition) in our calculations, thus, leads to a decrease in the RR intensity near the absorption maxima corresponding to the resonant electronic state. The displacements in dimensionless units for all of these Raman active vibrations are presented in Table 2, along with the parameters used to fit the REPs.

TABLE 2: Raman Frequencies, Experimental and Calculated (ω in cm^{-1}), Dimensionless Displacements (Δ) in the Resonant Electronic State, and the Potential Energy Distributions (PEDs) of *p*-Nitroazobenzene[a]

vibrational mode	ω (cm^{-1})		Δ	PEDs
	expt	cald		
υ_7	1602	1609	0.65	70υ(C−C), 19δ(C−C)
υ_8	1495	1495	0.94	61υ(C−C), 19δ(C−H)
υ_9	1473	1490	1.07	60υ(C−C), 19δ(C−H)
υ_{10}	1449	1418	1.07	45υ(N=N), 31υ(N−O)
υ_{12}	1413	1395	0.67	39υ(C−C), 25υ(N−O), 17υ(N=N)
υ_{13}	1348	1249	0.96	49υ(N−O), 30υ(C−N)$_{NO}$
υ_{15}	1180	1189	0.74	48υ(C-C), 48δ(C−H)
υ_{18}	1143	1146	1.26	34υ(C−N), 31δ(C−C), 19υ(C−C), 10δ(C−N)
υ_{19}	1109	1107	0.74	38υ(C−C), 34δ(C−C), 16υ(C−N)$_{NO}$

[a] Calculated frequencies obtained from B3LYP/6-31G and scaled by a factor of 0.97; υ = stretch; δ = in-plane bend; zero−zero energy, E_0 = 18 194.8 cm^{-1}; electronic transition dipole, M = 0.34 Å; lifetime broadening, Γ = 50 cm^{-1}; relaxation into different modes including bath, β = 750 cm^{-1}.

A comparative study of the experimental and the simulated absolute Raman intensities for all nine fundamental vibrations of *p*-nitroazobenzene are presented in Figure 5. For the sake of brevity, we present the results at a few excitation wavelengths, 443, 461, 480, and 501 nm. Here, we believe that the Raman fundamentals observed at 1602, 1495, 1473, and 1348 cm^{-1} are resonantly enhanced due to $^1(n \rightarrow \pi^*)$ excitation. The Raman excitation profiles corresponding to these fundamentals can also be fit by a single-state $^1(n \rightarrow \pi^*)$ enhancement model, and the calculated curve compares reasonably well with the experimental curve as shown in Figure 3. The singlet $^1(n \rightarrow \pi^*)$ enhancement model is also supported by the observation of very weak overtones and combination bands for these stretching vibrations at excitation wavelengths of 443 and 480 nm. The intensities of the overtones and combination bands are found to be very weak, that is, an order of magnitude lower than intensities for the fundamental vibrations. Moreover, the signal-to-noise ratio for the overtones and combination bands is poor, that is, within the error bar. The calculated intensities using the singlet-state enhancement model for the respective overtones are found to be 10−20 times lower in intensity as compared to the fundamental. These calculated intensities for the overtones (slashed bars) are also plotted in Figure 5 for the sake of comparison with the fundamental intensities. From Figure 5, it

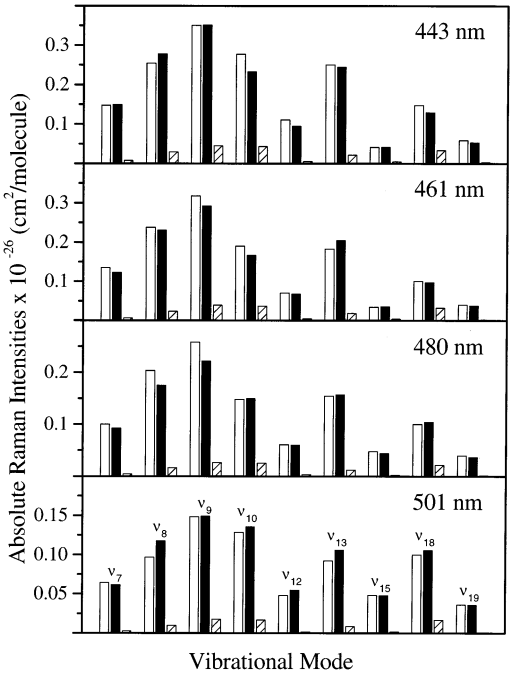

Figure 5. Comparison of the experimental (open bars) and calculated absolute Raman intensities for the fundamentals (solid bars) and the overtones (slashed bars) at excitation wavelengths 443, 461, 480, and 501 nm.

is seen that the calculated intensities for the overtones are an order of magnitude lower in intensity than the fundamentals and, hence, are consistent with the experimental observation. This gives good evidence that our assumption of a singlet-state enhancement model for these modes is valid. Moreover, the solid bars representing the calculated results exhibit a good description of the experimental Raman intensities for all of the fundamental vibrations at different excitation wavelengths, which are shown by open bars in the figure. This confirms that the assumptions considered for the simulations are reasonable.

The absorption spectrum for the $^1(n \rightarrow \pi^*)$ transition is modeled using eqs 1, 4, and 5. We use the Gaussian component obtained by deconvoluting the total absorption spectrum as shown in Figure 1 as the representation for the absorption spectrum corresponding to the $^1(n \rightarrow \pi^*)$ electronic transition. The fitting parameters required to simulate this absorption spectrum are identical to those used to simulate the REPs and are presented in Table 2. The experimental absorption spectrum, the Gaussian deconvoluted component, and the simulated spectra for the $^1(n \rightarrow \pi^*)$ transition are shown in Figure 6 by dots, solid line, and dashed line, respectively. It is evident that the simulated spectrum provides a good description of the experimental spectrum. The same set of parameters representing two completely different experimental results (viz., the REPs and the electronic absorption spectrum), thus, provides further support regarding the parameters used for the simulations.

D. Short-Time Isomerization Dynamics. On the basis of the simulation data, especially the dimensionless displacements along various fundamental vibrations as shown in Table 2, the isomerization dynamics of *p*-nitroazobenzene under $^1(n \rightarrow \pi^*)$ electronic excitation can be inferred. As observed from the table, the vibrational modes, namely, 1143, 1449, and 1473 cm^{-1}, have the largest displacements in the excited state. These modes are assigned to C−N, N═N, and C−C stretches, respectively. It is possible to envisage such large displacements for these modes when they participate in the isomerization dynamics. Thus, to acquire further information about the short-time isomerization

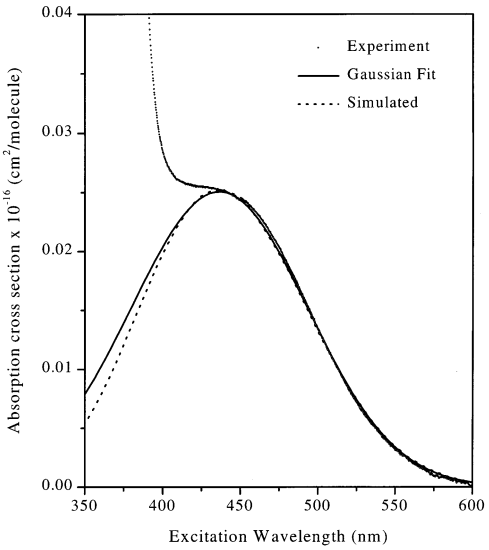

Figure 6. The experimental (dots), the Gaussian fit (solid line), and the simulated (dashed line) spectra for the $^1(n \rightarrow \pi^*)$ electronic transition of *p*-nitroazobenzene using the parameters of Table 2.

dynamics, a detailed study of normal coordinate analysis using density functional theory (B3LYP) with 6-31G basis set is carried out for *p*-nitroazobenzene.[66] Comparison of the experimental and theoretically calculated frequencies along with the calculated potential energy distributions (PEDs) for the observed fundamental vibrations are included in Table 2.

To get direct evidence for the isomerization pathway, namely, inversion or rotation, one would expect significant Raman activity in the corresponding fundamental mode or in the overtones for the corresponding inversion and torsional normal coordinates. From the density functional calculations using B3LYP with 6-31G basis set,[66] the N═N torsion and N-inversion mode (N−N bend) are expected around 40 and 940 cm^{-1}, respectively. The inversion mode is found to be very weak, while the N═N torsion is not observed in Raman. However, Rayleigh scattering usually strongly interferes at low frequencies, and unless the displacement is quite large along these coordinates, the overtones along these vibrations would not be observed. These modes were also not observed in the picosecond time-resolved Raman study of the S_1 state of *trans*-azobenzene,[69] and this was attributed to the fact that upon $^1(n \rightarrow \pi^*)$ excitation the π^* orbital is not just localized on the central N═N bond but it extends to the phenyl group and hence very small changes are observed around the N═N bond. Thus, we would like to give other evidences for understanding the isomerization pathway. The isomerization dynamics in *p*-nitroazobenzene upon $^1(n \rightarrow \pi^*)$ excitation can be inferred on the basis of the simulated dimensionless displacement parameters along the N═N, C−C, and C−N stretching vibrations for *p*-nitroazobenzene and azobenzene,[14d] and comparison of those with that of *trans*-stilbene[64] for which isomerization can occur only by rotation. In the case of *trans*-stilbene, the most intense Raman bands are observed at 1638 (interring ethylenic C═C stretch) and 1599 cm^{-1} (ring C═C stretch), followed by a moderately intense band at 1188 cm^{-1} (C−Ph stretch), where as in *p*-nitroazobenzene, maximum intensity, and hence displacement, is observed for the C−N ($\Delta = 1.26$), N═N ($\Delta = 1.07$), and ring C−C ($\Delta = 0.94$) stretching vibrations. The sharp contrast in the intensity and displacements of the C−Ph and the N−Ph vibrations in the two cases mentioned above gives evidence for isomerization via an inversion route under $^1(n \rightarrow \pi^*)$ electronic excitation in *p*-nitroazobenzene.

TABLE 3: Internal Coordinate Displacements of *p*-Nitroazobenzene at Various Times (*t*)

bonds	bond lengths (Å), bond angles (deg)[a]	*t* (fs) 10	20	30
N_1N_2	1.2790	0.0056	0.0217	0.0454
C_3N_1	1.4223	−0.0079	−0.0308	−0.0656
C_4N_2	1.4223	−0.0084	−0.0323	−0.0678
C_5C_3	1.4089	0.0046	0.0179	0.0377
C_6C_4	1.4089	0.0069	0.0264	0.0547
$C_{11}N_{21}$	1.4607	−0.0111	−0.0429	−0.0907
$N_{21}O_{25}$	1.2655	−0.0038	−0.0146	−0.0302
$N_{21}O_{26}$	1.2655	0.0158	0.0604	0.1261
$C_3N_1N_2$	115.7	0.0011	0.0043	0.0096
$C_4N_2N_1$	115.7	0.0001	0.0006	0.0020

[a] Calculated from B3LYP/6-31G

Thus, we believe that our conclusion about isomerization via nitrogen inversion is valid. This is supported by the picosecond time-resolved Raman study of the S_1 state on *trans*-azobenzene,[69] which gives a clear evidence that upon excitation from S_0 to the S_1 electronic state, there is significant shift in equilibrium geometry along various normal coordinates but not along the torsional coordinate.

From the knowledge of the ground-state normal mode description of *p*-nitroazobenzene at the equilibrium geometry, as well as the dimensionless displacements, and from employment of eqs 10−12, the change in internal coordinates as a function of time is calculated. The changes in the early times, namely, 10−30 fs, are only considered because the multimode correlation function decays within 30 fs. The RR intensity analysis only provides the magnitude but not the sign or direction of change of the FC active normal mode displacements. In reality, there are 2^n (*n* being the number of FC active modes) possible sign combinations that are equally consistent with the result of the RR intensity analysis. In the case of *p*-nitroazobenzene, there are 2^9 different possibilities for the sign combinations of the normal mode displacements. Of these 512 possible combinations, many involve physically unreasonable bond length and bond angle changes and, hence, can be easily ruled out. Among the remaining 33 possibilities, we have selected those that involve the direction of the geometry changes toward an inverted structure because upon $^1(n \rightarrow \pi^*)$ excitation of *p*-nitroazobenzene it is assumed that isomerization occurs via a linearly inverted transition state. Thus, during inversion, an electron moves from a nonbonding to an antibonding orbital leading to an elongation (change in positive direction) in the N═N bond length and NNC bond angles followed by a shortening (changes in negative direction) in the C−N bond lengths. Only 3 of the 33 possible sign combinations meet the above-mentioned constraints. Of these three, only one of the structures has the required geometry changes along the phenyl C−C bonds as is required for an inverted structure.[70] Hence, taking the latter sign combination for the dimensionless displacements of the observed normal vibrations, we have carried out the time-dependent structural dynamics. In Table 3, we have reported the changes in N_1═N_2, C_3−N_1, C_4−N_2, C_5−C_3, C_6−C_4, C_{11}−N_{21}, N_{21}−O_{25}, and N_{21}−O_{26} bond lengths and C_3−N_1−N_2 and C_4−N_2−N_1 bond angles at 10, 20, and 30 fs. The bond lengths[66] in angstroms and bond angles in degrees calculated from B3LYP with 6-31G basis set are also included in the table. It is observed from the table that the changes involved along N═N, C−N, C−C, and N−O stretching vibrations in *p*-nitroazobenzene within 30 fs are of the order of 0.05 to 0.1 Å, which is quite pronounced in a polyatomic system where the vibrations are all coupled and consists of contributions from various stretching and bending vibrations as shown from the calculated PEDs in Table 2.

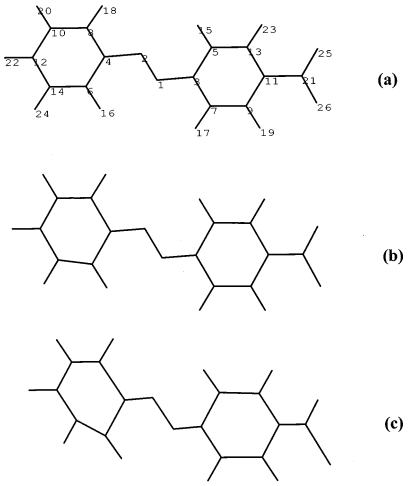

Figure 7. Schematic representation of *p*-nitroazobenzene isomerization dynamics at time (*t*) (a) 0, (b) 10, and (c) 20 fs. The magnitudes of displacement values are 10 times the true displacement.

In Figure 7, we have shown a schematic representation of the changes in *p*-nitroazobenzene at time (*t*) (a) 0, (b) 10, and (c) 20 fs. The magnitude of the displacements for 10 and 20 fs have been multiplied 10 times their true displacements for better visualization. The overall displacement at 10 and 20 fs visualizes the time evolution of the in-plane motions in *p*-nitroazobenzene because the normal mode vibrations observed under resonance excitation correspond mainly to the in-plane stretches and bends with little or no contribution from the out-of-plane vibrations. Thus, from the changes in displacements, we infer that upon $^1(n \rightarrow \pi^*)$ excitation in *p*-nitroazobenzene, isomerization occurs via inversion. Moreover, N═N and C−N stretching vibrations undergo considerable changes. It is observed from Figure 7 that the unsubstituted benzene ring undergoes significant distortion similar to the nitro group. Thus, it can be inferred that the N═N, C−N, C−C, and N−O stretching vibrations experience a considerable amount of distortion immediately upon photoexcitation.

Conclusions

Raman spectra are measured for *p*-nitroazobenzene dissolved in chloroform at 18 excitation wavelengths in resonance with the $^1(n \rightarrow \pi^*)$ electronic transition. It is observed that, while the REPs corresponding to the fundamental vibrations 1602, 1495, 1473, and 1348 cm^{-1} exhibit similar shape as that observed in the absorption spectrum, the REPs for the fundamentals 1449, 1413, 1180, 1143, and 1109 cm^{-1} show de-enhancement near the maxima of the $^1(n \rightarrow \pi^*)$ electronic transition. Resonance de-enhancement is attributed to interference from the strongly allowed $^1(\pi \rightarrow \pi^*)$ electronic state. We have used Heller's time-dependent wave packet dynamical approach for RR scattering to simulate the REPs for the FC active normal modes. The effect of interference due to the preresonant electronic state is included in our simulations of the REPs showing resonance de-enhancement. The experimental results (REPs and the absorption spectrum) can be consistently described within this theoretical model. The dimensionless displacements obtained from our calculation help in visualization of the isomerization dynamics in *p*-nitroazobenzene. It is observed that *p*-nitroazobenzene isomerizes via inversion upon photoexcitation to the $^1(n \rightarrow \pi^*)$ state. To visualize the short-time isomerization dynamics in *p*-nitroazobenzene, in terms of

bond length changes, the dimensionless displacements obtained from our simulations are converted with a priori knowledge of the accurate normal coordinate analysis. We find that during isomerization in *p*-nitroazobenzene, within a few femtoseconds, N═N and C−N bonds are affected considerably. It is also observed that the unsubstituted phenyl ring and the nitro stretching vibrations experience a noticeable amount of photoexcitation and hence are distorted significantly within 20 fs.

Acknowledgment. The authors thank the Council of Scientific and Industrial Research, the Department of Science and Technology, and the Jawaharlal Nehru Center for Advanced Scientific Research, Government of India, for financial assistance and the Supercomputer Education and Research Center of the Indian Institute of Science for providing the computing facilities necessary to carry out the present work. The authors also thank the reviewer for suggesting further refinement of the manuscript in terms of both presentation and scientific content.

References and Notes

(1) (a) Esposito, A. P.; Foster, C. E.; Beckman, R. A.; Reid, P. J. *J. Phys. Chem. A* **1997**, *101*, 5309. (b) Lawless, M. K.; Mathies, R. A. *J. Chem. Phys.* **1994**, *100*, 2492.

(2) (a) Sension, R. J.; Brudzynski, R. J.; Hudson, B. S.; Zhang, J.; Imre, D. G. *Chem. Phys.* **1990**, *141*, 393. (b) Sension, R. J.; Strauss, H. L. *J. Chem. Phys.* **1986**, *85*, 3791.

(3) (a) Morikis, D.; Li, P.; Bangcharoenpaurpong, O.; Sage, J. T.; Champion, P. M. *J. Phys. Chem.* **1991**, *95*, 3391. (b) Schomacker, K. T.; Champion, P. M.; Albrecht, A. C. *J. Chem. Phys.* **1986**, *84*, 5314. (c) Stallard, B. R.; Callis, P. R.; Champion, P. M.; Albrecht, A. C. *J. Chem. Phys.* **1984**, *80*, 70.

(4) (a) Wang, P. G.; Ziegler, L. D. *J. Chem. Phys.* **1991**, *95*, 288. (b) Ziegler, L. D.; Chung, Y. C.; Wang, P. G.; Zhang, Y. P. *J. Phys. Chem.* **1990**, *94*, 3394.

(5) (a) Amstrup, B.; Langkilde, F. W.; Bajdor, K.; Wilbrandt, R. *J. Phys. Chem.* **1992**, *96*, 4794. (b) Langkilde, F. W.; Wilbrandt, R.; Brouwer, A. M.; Jacobs, H. J. J.; Negri, F.; Orlandi, G. *J. Phys. Chem.* **1992**, *96*, 64.

(6) Kiefer, W.; Ganz, M.; Vogt, P.; Schmitt, M. *J. Mol. Struct.* **1995**, *347*, 229.

(7) Phillips, D. L.; Zgierski, M. Z.; Myers, A. B. *J. Phys. Chem.* **1993**, *97*, 1800.

(8) (a) Zheng, X.; Phillips, D. L. *J. Chem. Phys.* **1999**, *110*, 1638. (b) Lilichenko, M.; Tittelbach-Helmrich, D.; Verhoeven, J. W.; Gould, I. R.; Myers, A. B. *J. Chem. Phys.* **1998**, *109*, 10958.

(9) Sweeney, J. A.; Asher, S. A. *J. Phys. Chem.* **1990**, *94*, 4784.

(10) Shin, K.-S.; Clark, R. J. H.; Zink, J. I. *J. Am. Chem. Soc.* **1989**, *111*, 4244.

(11) Myers, A. B.; Mathies, R. A. In *Biological Applications of Raman Spectroscopy*; Spiro, T. G., Ed.; John Wiley and Sons, Inc.: New York, 1987; Vol. 2, p 1.

(12) Zink, J. I.; Shin, K.-S. K. *Advances in Photochemistry*; John Wiley and Sons, Inc.: New York, 1991; Vol. 16, p 119.

(13) Myers, A. B. In *Laser Techniques in Chemistry*; Myers, A. B., Rizzo, T. R., Eds.; John Wiley and Sons, Inc.: New York, 1995; Vol 23, p 325.

(14) (a) Biswas, N.; Umapathy, S.; Kalyanaraman, C.; Sathyamurthy, N. *Proc. − Indian Acad. Sci., Chem. Sci.* **1995**, *107*, 233. (b) Biswas, N.; Umapathy, S. *Curr. Sci.* **1998**, *74*, 328. (c) Biswas, N.; Umapathy, S. *J. Chem. Phys.* **1997**, *107*, 7849. (d) Biswas, N.; Umapathy, S. *Chem. Phys. Lett.* **1995**, *234*, 24. (e) Biswas, N.; Umapathy, S. *Appl. Spectrosc.* **1998**, *52*, 496. (f) Biswas, N. Resonance Raman Studies on Structure and Dynamics of Azobenzene and its Derivatives. Ph.D. Dissertation, Department of Inorganic and Physical Chemistry, Indian Institute of Science, Bangalore, India, 1998.

(15) (a) Phillips, D. L.; Myers, A. B. *J. Chem. Phys.* **1991**, *95*, 226. (b) Markel, F.; Myers, A. B. *J. Chem. Phys.* **1993**, *98*, 21.

(16) (a) Lee, S.-Y.; Heller, E. J. *J. Chem. Phys.* **1979**, *71*, 4777. (b) Heller, E. J. *J. Chem. Phys.* **1975**, *62*, 1544. (c) Heller, E. J. *Acc. Chem. Res.* **1981**, *14*, 368.

(17) Albrecht, A. C.; Hutley, M. C. *J. Chem. Phys.* **1971**, *55*, 4438.

(18) Albrecht, A. C. *J. Chem. Phys.* **1961**, *34*, 1476.

(19) Clark, R. J. H.; Dines, T. J. *Angew Chem., Int. Ed. Engl.* **1986**, *25*, 131.

(20) Schick, G. A.; Bocian, D. F. *J. Raman Spectrosc.* **1981**, *11*, 27.

(21) Nafie, L. A.; Pastor, R. W.; Dabrowiak, J. C.; Woodruff, W. H. *J. Am. Chem. Soc.* **1976**, *98*, 8007.

(22) (a) Fodor, S. P. A.; Copeland, R. A.; Grygon, C. A.; Spiro, T. G. *J. Am Chem Soc.* **1989**, *111*, 5509. (b) Bosworth, Y. M.; Clark, R. J. H. *J. Chem. Soc., Dalton Trans.* **1974**, 1749. (c) Bosworth, Y. M.; Clark, R. J. H.; Turtle, P. C. *J. Chem. Soc., Dalton Trans.* **1975**, 2027.

(23) (a) Stein, P.; Miskowski, V.; Woodruff, W. H.; Griffin, J. P.; Werner, K. G.; Gaber, B. P.; Spiro, T. G. *J. Chem. Phys.* **1976**, *64*, 2159. (b) Johnson, B. B.; Peticolas, W. L. *Annu. Rev. Phys. Chem.* **1976**, *27*, 465. (c) Spiro, T. G.; Stein, P. *Annu. Rev. Phys. Chem.* **1977**, *28*, 501.

(24) (a) Zgierski, M. Z. *J. Raman Spectrosc.* **1977**, *6*, 53. (b) Zgierski, M. Z. *J. Raman Spectrosc.* **1976**, *5*, 181.

(25) Korenowski, G. M.; Ziegler, L. D.; Albrecht, A. C. *J. Chem. Phys.* **1978**, *68*, 1248.

(26) Asher, S. A.; Johnson, C. R. *J. Phys. Chem.* **1985**, *89*, 1375.

(27) Hildebrandt, P.; Tsuboi, M.; Spiro, T. G. *J. Phys. Chem.* **1990**, *94*, 2274.

(28) Siebrand, W.; Zgierski, M. Z. *J. Chem. Phys.* **1979**, *71*, 3561.

(29) (a) Rimai, L.; Heyde, M. E.; Heller, H. C.; Gill, D. *Chem. Phys. Lett.* **1971**, *10*, 207. (b) Friedman, J.; Hochstrasser, R. M. *Chem. Phys. Lett.* **1975**, *32*, 414.

(30) Shin, K.-S. K.; Zink, J. I. *J. Am. Chem. Soc.* **1990**, *112*, 7148.

(31) Reber, C.; Zink, J. I. *J. Phys. Chem.* **1992**, *96*, 571.

(32) Sztainbuch, I. W.; Leroi, G. E. *J. Chem. Phys.* **1990**, *93*, 4642.

(33) Biswas, N.; Umapathy, S. *Pramana J. Phys.* **1997**, *48*, 937.

(34) (a) Bach, H.; Anderle, K.; Fuhrmann, Th.; Wendorff, J. H. *J. Phys. Chem.* **1996**, *100*, 4135. (b) Liu, Z.; Zhao, C.; Tang, M.; Cai, S. *J. Phys. Chem.* **1996**, *100*, 17337.

(35) (a) Ramanujam, P. S.; Hvilsted, S.; Andruzzi, F. *Appl. Phys. Lett.* **1993**, *62*, 1041. (b) Ramanujam, P. S.; Hvilsted, S.; Zebger, I.; Siesler, H. W. *Macromol. Rapid Commun.* **1995**, *16*, 455. (c) Hvilsted, S.; Andruzzi, F.; Ramanujam, P. S. *Opt. Lett.* **1992**, *17*, 1234.

(36) Lee, G. J.; Kim, D.; Lee, M. *Appl. Opt.* **1995**, *34*, 138.

(37) Willner, I.; Rubin, S. *Angew. Chem., Int. Ed. Engl.* **1996**, *35*, 367.

(38) Eich, M.; Wendorff, J. H. *Makromol. Chem. Rapid Commun.* **1987**, *8*, 467; *J. Opt. Soc. Am. B: Opt. Phys.* **1990**, *7*, 1428.

(39) Eich, M.; Wendorff, J. H.; Reck, B.; Ringsdorf, H. *Makromol. Chem. Rapid Commun.* **1987**, *8*, 59.

(40) Anderle, K.; Birenheide, B.; Eich, M.; Wendorff, J. H. *Makromol. Chem. Rapid Commun.* **1989**, *10*, 477.

(41) Natansohn, A.; Rochon, P.; Gosselin, J.; Xie, S. *Macromolecules* **1992**, *25*, 2268.

(42) Todorov, T.; Nikolova, L.; Tomova, N. *Appl. Opt.* **1984**, *23*, 4309.

(43) Ikeda, T.; Tsutsumi, O. *Science* **1995**, *268*, 1873.

(44) Sekkat, Z.; Dumont, M. *Appl. Phys. B* **1992**, *54*, 486.

(45) Liu, Z. F.; Hashimoto, K.; Fujishima, A. *Nature* **1990**, *347*, 658.

(46) Ulysse, L.; Cubillos, J.; Chmielewski, J. *J. Phys. Chem.* **1995**, *117*, 8466.

(47) Kumar, G. S.; Neckers, D. C. *Chem. Rev.* **1989**, *89*, 1915.

(48) Rau, H. In *Photochromism. Molecules and Systems*; Durr, H., Bouas-Laurent, H., Eds.; Elsevier: Amsterdam, 1990; Chapter 4, p 165.

(49) (a) Rau, H.; Luddecke, E. *J. Am. Chem. Soc.* **1982**, *104*, 1616. (b) Rau, H. *J. Photochem.* **1984**, *26*, 221. (c) Rau, H.; Yu-Quan, S. J. *J. Photochem. Photobiol. A: Chem.* **1988**, *42*, 321.

(50) (a) Struve, W. S. *Chem. Phys. Lett.* **1977**, *46*, 15. (b) Morgante, C. G.; Struve, W. S. *Chem. Phys. Lett.* **1979**, *68*, 267. (c) Asano, T.; Okada, T.; Shinkai, S.; Shigematsu, K.; Kusano, Y.; Manabe, O. *J. Am. Chem. Soc.* **1981**, *103*, 5161.

(51) Lednev, I. K.; Ye, T.-Q.; Hester, R. E.; Moore, J. N. *J. Phys. Chem.* **1996**, *100*, 13338.

(52) Hamm, P.; Ohline, S. M.; Zinth, W. *J. Chem. Phys.* **1997**, *106*, 519.

(53) Okamoto, H.; Hamaguchi, H.; Tasumi, M. *Chem. Phys. Lett.* **1986**, *130*, 185.

(54) Monti, S.; Orlandi, G.; Palmieri, P. *Chem. Phys.* **1982**, *71*, 87.

(55) Lunak, S., Jr.; Nepras, M.; Hrdina, R.; Mustroph, H. *Chem. Phys.* **1994**, *184*, 255.

(56) Rau, H. *Angew. Chem., Int. Ed. Engl.* **1973**, *12*, 224.

(57) Myers, A. B.; Li, B.; Ci, X. *J. Chem. Phys.* **1988**, *89*, 1876.

(58) Womack, J. D.; Mann, C. K.; Vickers, T. J. *Appl. Spectrosc.* **1989**, *43*, 527.

(59) Feit, M. D.; Fleck, J. A., Jr.; Steiger, A. *J. Comput. Phys.* **1982**, *47*, 412.

(60) (a) Kosloff, R. *J. Phys. Chem.* **1988**, *92*, 2087. (b) Williams, S. O.; Imre, D. G. *J. Phys. Chem.* **1988**, *92*, 3363.

(61) Trulson, M. O.; Mathies, R. A. *J. Chem. Phys.* **1986**, *84*, 2068.

(62) Jaffe, H. H.; Orchin, M. *Theory and applications of ultraviolet spectroscopy*; John Wiley and Sons, Inc.: New York, 1962; Chapter 15, p 430.

(63) Marconi, G.; Houben, J. *J. Chem. Soc., Faraday Trans. 2* **1985**, *81*, 975.

(64) Myers, A. B. Ph.D. Dissertation, University of California, Berkeley, Berkeley, CA, 1984.

(65) Wilson, E. B., Jr.; Decius, J. C.; Cross, P. C. *Molecular Vibrations*; Dover: New York, 1980.

(66) Biswas, N.; Umapathy, S. *J. Phys. Chem. A* **2000**, *104*, 2734.
(67) Frisch, M. J.; Trucks, G. W.; Schlegel, H. B.; Gill, P. M. W.; Johnson, B. G.; Robb, M. A.; Cheeseman, J. R.; Keith, T.; Petersson, G. A.; Montgomery, J. A.; Raghavachari, K.; Al-Laham, M. A.; Zakrzewski, V. G.; Ortiz, J. V.; Foresman, J. B.; Cioslowski, J.; Stefanov, B. B.; Nanayakkara, A.; Challacombe, M.; Peng, C. Y.; Ayala, P. Y.; Chen, W.; Wong, M. W.; Andres, J. L.; Replogle, E. S.; Gomperts, R.; Martin, R. L.; Fox, D. J.; Binkley, J. S.; Defrees, D. J.; Baker, J.; Stewart, J. P.; Head-Gordon, M.; Gonzalez, C.; Pople, J. A. *Gaussian 94*, revision C.2; Gaussian, Inc.: Pittsburgh, PA, 1995.
(68) (a) Biswas, N.; Umapathy, S. *J. Phys. Chem. A* **1997**, *101*, 5555. (b) Mohandas, P.; Umapathy, S. *J. Phys. Chem. A* **1997**, *101*, 4449.
(69) Fujino, T.; Tahara, T. *J. Phys. Chem. A* **2000**, *104*, 4203.
(70) Catteneo, P.; Persico, M. *Phys. Chem. Chem. Phys.* **1999**, *1*, 4739.